Peter Mayr[a], Todd A. Palmer[b], John W. Elmer[b], Eliot D. Specht[c]
[a] Graz University of Technology, IWS, Graz, Austria
[b] Lawrence Livermore National Laboratory, Livermore, USA
[c] Oak Ridge National Laboratory, Oak Ridge, USA

Direct observation of phase transformations in the simulated heat-affected zone of a 9Cr martensitic steel

An experimental test melt of a boron alloyed 9Cr-3W-3Co-V,Nb steel for high temperature applications in the thermal power generation industry was produced by vacuum induction melting. This grade of steel typically displays a homogeneous tempered martensitic microstructure in the as-received, i.e. normalised and tempered, condition. However, after welding, this microstructure is significantly altered, resulting in a loss of its desired properties. The phase transformations during simulated thermal cycles typical of those experienced in the weld heat-affected zone were directly observed by in-situ X-ray diffraction experiments using synchrotron radiation. Heating rates of $10\,K\,s^{-1}$ and $100\,K\,s^{-1}$ up to a peak temperature of 1300 °C are investigated here. The final microstructures observed after both simulated weld thermal cycles are primarily composed of martensite with approximately 4 % retained delta ferrite and 4 % retained austenite, by volume. With the temporal resolution of the in-situ X-ray diffraction technique, phase transformations from tempered martensite to austenite to delta ferrite during heating and to martensite during cooling were monitored. With this technique, the evolution of the final microstructure through both heating and cooling is monitored, providing additional context to the microstructural observations.

Keywords: Chromium steels; Heat-affected zone; Phase transformations; Delta ferrite; Retained austenite

1. Introduction

Martensitic 9–12 wt.% chromium steels with controlled additions of boron and nitrogen have received increased interest for high temperature applications in the thermal power generation industry [1–5]. These steels are processed using a complex heat treatment procedure to create a fully martensitic microstructure with finely dispersed $M_{23}C_6$ and MX type precipitates located along prior austenite grain boundaries as well as martensitic lath and subgrain boundaries [6, 7]. This combination of microstructural constituents ensures a high resistance to creep up to temperatures of 620 °C.

These 9–12 wt.% Cr steels primarily solidify with either a fully ferritic (delta ferrite – δ) or a dual austenite (γ) and delta ferrite (δ) microstructure. The presence of δ-ferrite in these martensitic steels has been shown to reduce their toughness and ductility [8–10], creep rupture strength [11–14], low cycle fatigue and creep fatigue strength [15, 16], and oxidation resistance [17]. Therefore, the elimination of the retained δ-ferrite by a balanced alloying concept and a sound heat treating procedure is one of the main targets in the development of martensitic steels.

Thermal cycles typical of welding and post-weld heat treating significantly alter this carefully adjusted microstructure. The heat-affected zone (HAZ) of these martensitic steels is characterised by a very complex structure and consists of several sub-zones displaying different microstructural features [18–20]. Regions close to the weld fusion line are exposed to high peak temperatures and can contain significant amounts of retained delta ferrite after welding.

An understanding of the phase transformations that occur during characteristic weld thermal cycles is important for a better understanding of the microstructural evolution in these regions. By using conventional dilatometry, the onset of austenite formation (A_{C1}), its completion (A_{C3}) on heating, and the martensite start temperature (M_S) on cooling can be determined from changes in the expansion of the sample. Dilatometry, though, is not well suited to monitoring the transformation of austenite to delta ferrite (A_{C4}) and its retransformation in the high temperature region.

In-situ X-ray diffraction (XRD) using high energy synchrotron radiation has been successfully employed for the characterisation of phase transformations in a range of materials systems [21–28]. Comprehensive maps of phases existing in the HAZ during welding have been produced for 1005 steel [22, 24], 1045 steel [28], titanium [21], and duplex stainless steel [23] based on in-situ XRD. The effects of the welding process on the delta ferrite–austenite phase balance in the steel welds across all of the HAZ regions surrounding the weld pool were studied, including the formation of bainite and martensite [25] on cooling at high rates. The effects of weld heat input on the size of the different HAZ was studied in 1045 steel [26], including mechanisms for the ferrite to austenite transformation on heating [27].

In the work presented here, an in-situ synchrotron X-ray diffraction technique is used to monitor phase transformations occurring during controlled heating and cooling of a

MK_mk101649 – 21.2.08/druckhaus köthen

Table 1. Chemical composition of 9Cr-3W-3Co-V,Nb test melt in wt.% balance Fe.

Analysis	C	Si	Mn	Cr	W	Co	V	Nb	B	N
	0.074	0.29	0.44	9.26	2.84	2.95	0.21	0.056	0.0120	0.0130

complex martensitic 9 wt.% chromium steel. These heating and cooling cycles are designed to simulate the thermal cycles typically experienced in the weld HAZ. Through these experiments, the formation of austenite and delta ferrite on heating are monitored and characterised, as is the evolution of the martensitic microstructure during cooling. The origin of the retained austenite and delta ferrite observed in HAZ microstructures is also analysed.

2. Experimental

A 20 kg test melt of a 9Cr-3W-3Co-V,Nb steel with controlled additions of 120 ppm boron and 130 ppm nitrogen was produced by vacuum induction melting. The exact chemical composition in wt.% of the test melt is given in Table 1. For homogenisation of the material, the ingot (110 mm square) was forged within a temperature window of 950 °C – 1150 °C to final dimensions of 50 mm square. The final quality heat treatment consisted of normalising at 1150 °C for 1 hour followed by tempering at 780 °C for 4 h.

Metallographic specimens were sectioned from the small ingot, polished to a 1 μm finish, and etched using a prior austenite grain boundary sensitive modified LBII aqueous solution containing 0.75 g/100 ml ammonium hydrogen fluoride and 0.9 g/100 ml potassium disulphide. After normalising and tempering, the steel shows a homogeneous tempered martensitic microstructure with precipitates aligned along prior austenite grain boundaries and martensite lath boundaries (Fig. 1). No delta ferrite was observed in the as-received condition. The prior austenite grains of the starting material have an equivalent average diameter of 250 μm.

The in-situ X-ray diffraction experiments were performed at the UNICAT beamline BM-33-C at the Advanced Photon Source (APS), Argonne, USA using a 30 keV X-ray beam. The monochromatised beam was focused and sized to dimensions of 1 mm wide by 0.25 mm high using a dynamically bent Si crystal and collimator slits. Test coupons measuring 100 mm long by 4.75 mm wide by 2 mm thick were machined from the base material bar and used in these experiments. The surface of the sample was polished using metallographic methods to a 1 μm finish where the X-ray impinges in preparation for the XRD experiments.

Direct resistance heating of the sample was used to apply a thermal cycle, and water cooled grips allowed the sample to be rapidly cooled. The temperature of the sample was monitored and recorded using type-S (Pt-Pt/Rh) thermocouples which were spot welded on the back side of the sample directly below the X-ray impingement point. A schematic of the experimental setup is shown in Fig. 2. Further details regarding the experimental setup are described in detail elsewhere [29].

Two thermal cycles were investigated within this work. The slower thermal cycle consisted of heating to a peak temperature of 1300 °C at a rate of 10 K s^{-1}. After holding at the peak temperature for 3 s, the sample was allowed to cool freely to room temperature which resulted in a characteristic cooling time between 800 °C and 500 °C ($t_{8/5}$-time) of approximately 40 s. The faster thermal cycle was characterised by a heating rate of 100 K s^{-1} up to a peak temperature of 1300 °C. Holding time at peak temperature and cooling rate were similar to the slower thermal cycle. Each sample, along with the heating and cooling stage assembly, was placed inside a vacuum chamber in order to minimise any potential oxidation and atmospheric contamination during the heating cycles. Prior to the experiment, the chamber was evacuated and maintained under vacuum during the entire experiment.

The samples were scanned in the *d*-spacing range of 1.1 to 2.3 Å, allowing three Debye arcs representing the austenite phase and three arcs representing the ferrite/martensite

Fig. 1. Optical micrograph of base material in normalised and tempered condition showing a tempered martensitic microstructure.

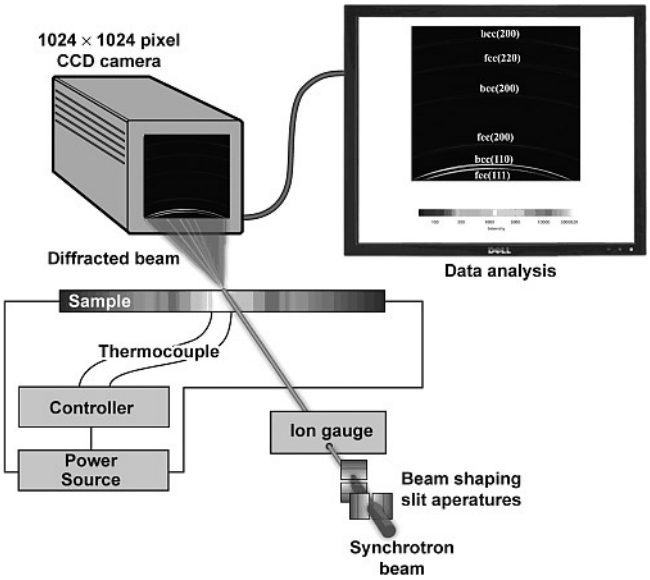

Fig. 2. Schematic of the experimental setup for in-situ X-ray diffraction experiments using synchrotron radiation during direct resistance heating of specimens.

phase to be monitored. During the XRD runs, diffraction patterns were captured with a one second exposure of a CCD camera, followed by a two second rest period for the bins in the CCD detector to be cleared. Therefore, patterns could only be taken at three second intervals. The Debye arcs were then converted into a 1-D plot showing diffracted beam intensity versus *d*-spacing using Fit-2D software [30]. Because of their similar lattice constants, the diffraction peaks of the ferrite (body-centred-cubic – bcc) and martensite (body-centred tetragonal – bct) [31] phases cannot be distinguished by this technique.

The phase fractions of delta ferrite and newly formed martensite are combined to give an integrated ferrite/martensite phase fraction. The amounts of austenite and ferrite/martensite present at each time increment are then calculated using an analysis of the peaks present in each diffraction pattern and plotted as a function of temperature. A detailed description of the method is given elsewhere [24].

Dissolution of precipitates and local enrichment in alloying elements were investigated using a Leo 1450 VP scanning electron microscope equipped with an Everhard-Thornley 4-quadrant backscatter detector and line scans using an attached Bruker X-Flash 4010 energy dispersive X-ray (EDX) detector.

3. Results and discussion

3.1. In-situ X-ray diffraction experiments

In-situ X-ray diffraction techniques were used to directly observe changes in the crystal structure of this 9 % chromium steel and to measure the relative amounts of martensite, austenite and delta ferrite under controlled heating and cooling conditions typical of that experienced in the weld HAZ. Figure 3 shows the diffraction patterns obtained at room temperature (a), at 1016 °C (b) and close to the peak temperature at 1295 °C (c) with a heating rate of 10 K s^{-1}. In the initial stage of heating, only bcc peaks of the tempered martensite are present (Fig. 3a). Whereas, at a temperature of 1016 °C only peaks of the face-centred cubic (fcc) austenite are recorded, indicating that the tempered martensite has fully transformed and the steel has been austenitised. Close to the peak temperature of 1300 °C, bcc peaks reappear, indicating the formation of high temperature delta ferrite.

The intensity plots in Fig. 4. follow the progression of the bcc(110) and fcc(111) peaks over the course of the simulated thermal cycle in each experiment. The measured specimen temperature is also shown to the right of each intensity plot. During the initial stage of heating, the bcc *d*-spacing values increase as a result of thermal expansion. The ferrite to austenite transformation then proceeds very rapidly, starting at a temperature of approximately 900 °C, and ending at a temperature of approximately 1016 °C. Only a sharp transition to the higher fcc *d*-spacing is visible. Further increases in temperature lead to the thermal expansion of the austenitic lattice until transformation to delta ferrite is initiated with the reappearance of the bcc(110) peak and a decrease in the intensity of the austenite peaks. The sequence of phase transformations observed during the faster thermal cycle is basically the same. At the high heating rate (100 K s^{-1}), though, the fully austenitised condition is passed through on heating very quickly and few diffraction patterns are obtained within the austenite single phase region.

During cooling, delta ferrite transforms back to austenite but never reaches completion, as evidenced by a remaining weak trace of the ferrite signal. After reaching a certain temperature (~420 °C), the intensity of the austenite peak begins to decrease and the intensity of the ferrite peak increases, indicating the onset of martensite formation (M_S-martensite start temperature). The exothermic nature of the transformation of austenite to martensite leads to a decrease in cooling rate during the time interval of martensitic transformation. Similar behaviour is observed for both thermal cycles.

In Fig. 5, the phase fractions are plotted as a function of temperature for both thermal cycles. Starting from a tempered martensitic microstructure, the steel fully transforms to austenite during heating. As also shown in the single diffraction patterns, the steel at higher temperatures enters a dual phase region of austenite and delta ferrite. Shortly after reaching the peak temperature, the delta ferrite reaches a maximum. During cooling, the phase fraction of delta fer-

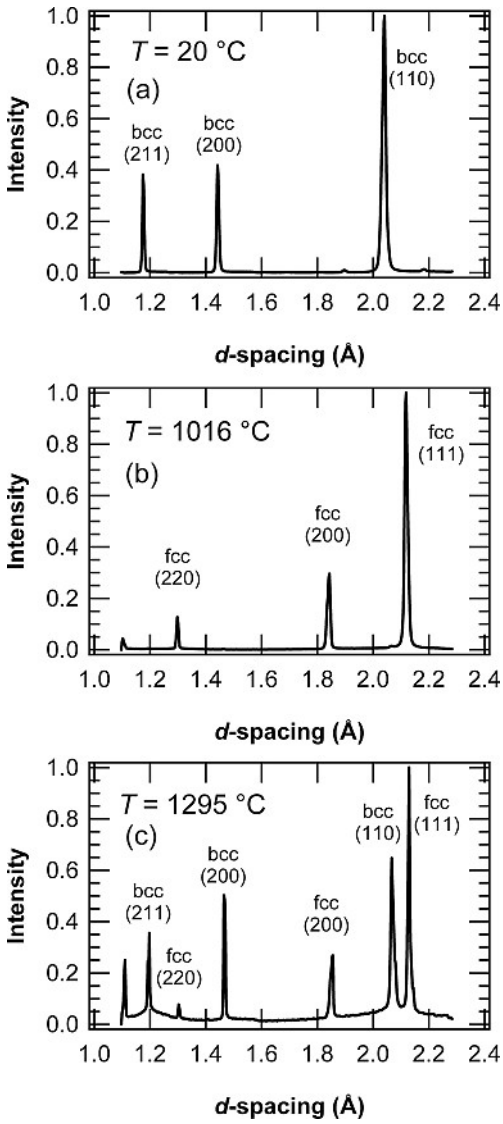

Fig. 3. Diffraction patterns recorded at different temperatures during the slow thermal cycle (10 K s^{-1}): (a) initial diffraction pattern at ambient temperature, (b) fully austenitised at 1016 °C, and (c) close to the peak temperature at 1295 °C.

rite steadily decreases while the austenite fraction increases. The phase fraction of ferrite does not completely transform to austenite on cooling.

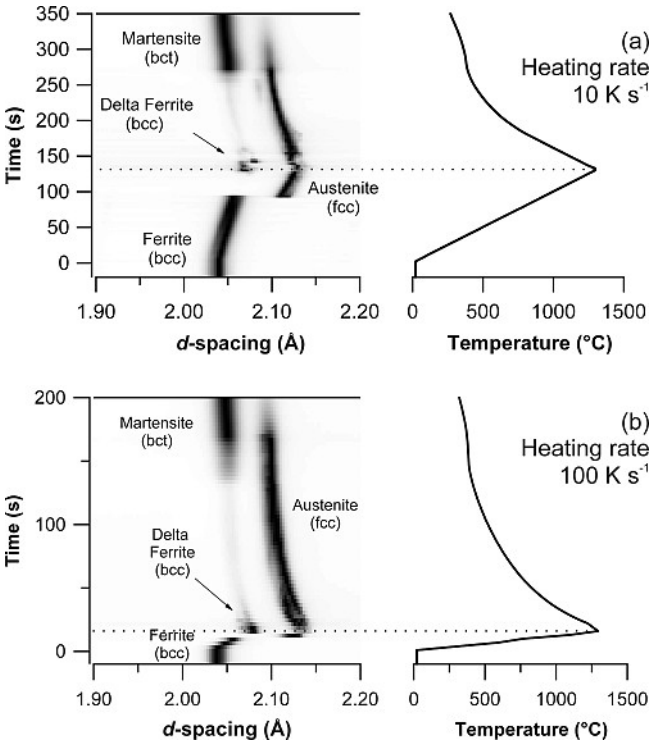

Fig. 4. Sequence of phase transformations in 9Cr-3W-3Co-V, Nb steel for a thermal cycle with a heating rate of (a) 10 K s^{-1} and (b) 100 K s^{-1} observed by in-situ X-ray diffraction experiments using synchrotron radiation.

As the steel has been fully austenitised on heating (see diffraction pattern in Fig. 3b), the measured bcc peaks close to the peak temperature originate only from the volume fraction of delta ferrite and not from the initial tempered martensitic microstructure. Approximately 4 % of delta ferrite is retained through the initial portions of the cooling cycle. At a temperature of about 430 °C, austenite starts to transform to martensite. A slight decrease in the cooling rate is observed at this same temperature, resulting from the exothermic nature of the martensitic transformation. It is assumed that the d-ferrite present at the initiation of the martensitic transformation remains in the microstructure and is included in the resulting phase fraction measurements. After completion of the fast thermal cycle, the HAZ simulated microstructure consists primarily of virgin martensite with approximately 4 % retained delta ferrite and 4 % retained austenite. Further cooling of the HAZ simulated microstructure by immersing the sample into liquid nitrogen did not result in a transformation of the retained austenite into martensite indicating that austenite is a stable constituent in this microstructure.

The experimental results, particularly those obtained at the lower heating rate, allowed for the determination of phase transformation temperatures signifying the onset of the ferrite to austenite transformation (A_{C1}), its completion (A_{C3}), the onset of delta ferrite formation (A_{C4}), and the martensite start temperature (M_S). Since the experimental setup for the diffraction measurements is characterised by a time resolution of 3 s, the exact temperature of the onset of each phase transformation is appointed with some level of uncertainty. Therefore, the temperature interval in which the phase transformation starts is given. The temperature intervals of the transformations are summarised in Table 2.

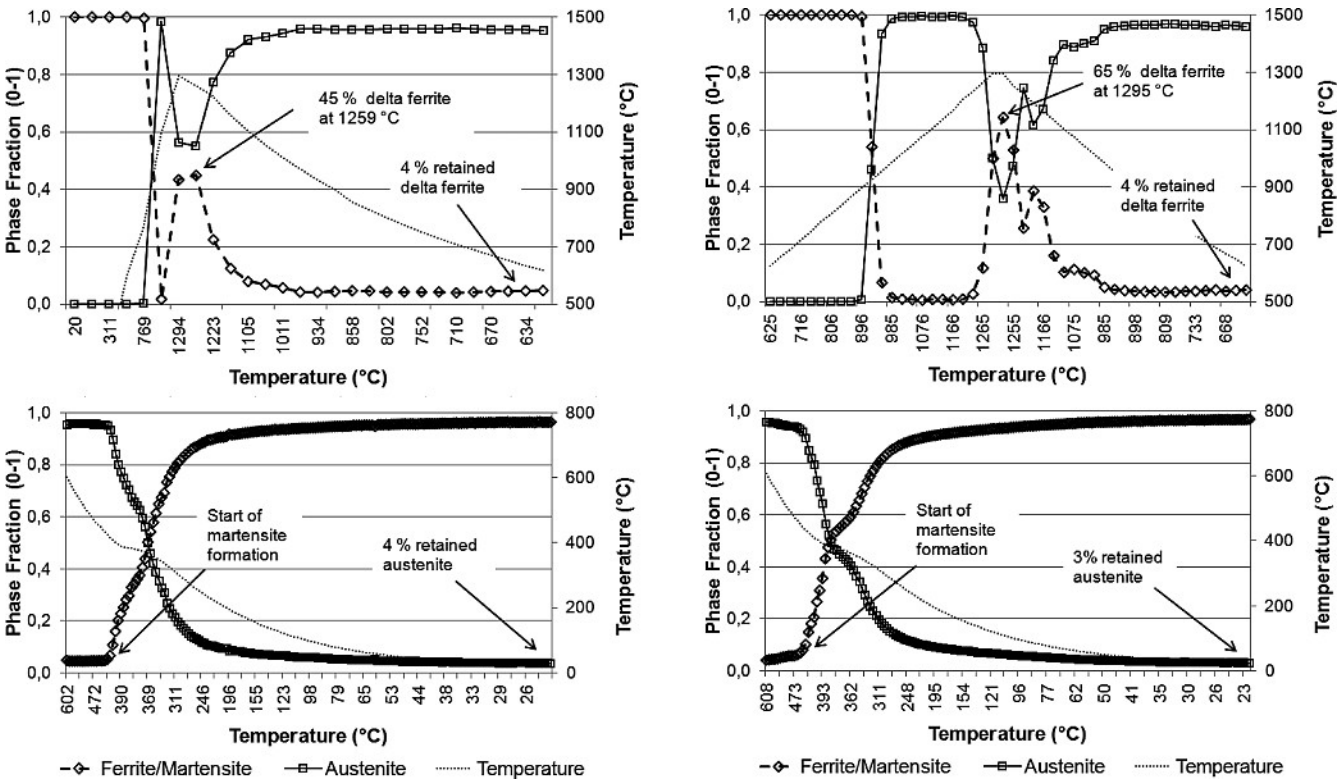

Fig. 5. Plots of the volume fractions of the matrix phases, ferrite/martensite and austenite, during the initial heating and cooling part (top) and the further cooling down to room temperature (bottom) evaluated from XRD data of the thermal cycles with a heating rate of 100 K s^{-1} (left) and 10 K s^{-1}(right).

Table 2. Temperature intervals of the onset of phase transformations and final microstructures measured for two different thermal cycles by in-situ X-ray diffraction.

Specimen	Heating rate ($K\ s^{-1}$)	A_{C1} (°C)	A_{C3} (°C)	A_{C4} (°C)	M_S (°C)	Maximum δ-ferrite (%)	Final microstructure
(N1)	100	n. o.	n. o.	n. o.	424 – 433	45 %	martensite 4 % δ-ferrite 4 % austenite
(N5)	10	896 – 924	985 – 1016	1206 – 1235	443 – 446	65 %	martensite 4 % δ-ferrite 3 % austenite

n. o. … not obtained due to high heating rate

Specifically, above the A_{C4} transformation temperature, δ-ferrite starts to nucleate and grows by a diffusive process. The slower thermal cycle allows the sample to be exposed to temperatures above the A_4 temperature for a long period of time, thus explaining the higher maximum δ-ferrite content of 65 % produced by the slower thermal cycle compared to the 45 % of the faster thermal cycle. Interestingly, the levels of retained delta ferrite (4 %) and austenite (3 to 4 %) after completion of the thermal simulation are very similar for both temperature cycles.

Optical microscopy was used to reveal the microstructures found after each experiment. Figure 6 shows optical micrographs of the resulting microstructure after HAZ simulation for both heating rates.

The retained delta ferrite appears as bright phase between the packages of martensite laths. Local enrichment in chromium resulting from the dissolution of chromium rich $M_{23}C_6$ particles and also tungsten was detected by an EDX line scan across a delta ferrite region, as shown in a backscattered electrons image (Fig. 7). This enrichment is high enough to allow the delta ferrite to remain stable at room temperature and is also supported by optical microscopy, which shows δ-ferrite grains at the prior location of the chromium carbides. Retained austenite could not be visualised by microscopy.

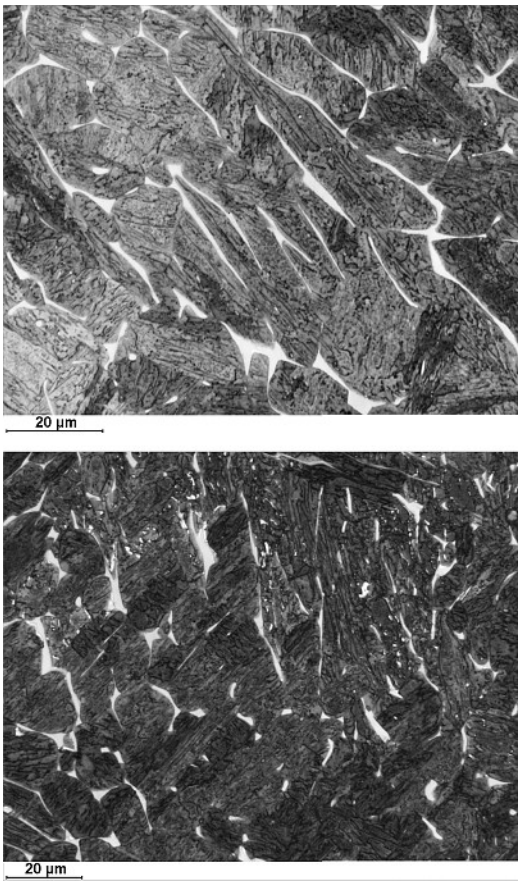

Fig. 6. Optical micrographs of weld simulated HAZ microstructure with a peak temperature of 1300 °C applying a heating rate of 10 $K\ s^{-1}$ (top) and 10 $K\ s^{-1}$ (bottom).

4. Summary and conclusions

Phase transformations in a 9Cr-3W-3Co-V, Nb steel with controlled additions of boron and nitrogen were observed using in-situ X-ray diffraction using synchrotron radiation during simulated HAZ heating and cooling cycles. This experimental method provides detailed insight into the important phase transformations in the HAZ of a martensitic chromium steel. Based on these results, a number of specific conclusions can be drawn.

1. During the entire thermal cycle, four phase transformations are observed. During heating at a rate of 10 $K\ s^{-1}$, the onset of austenite formation from the initial tem-

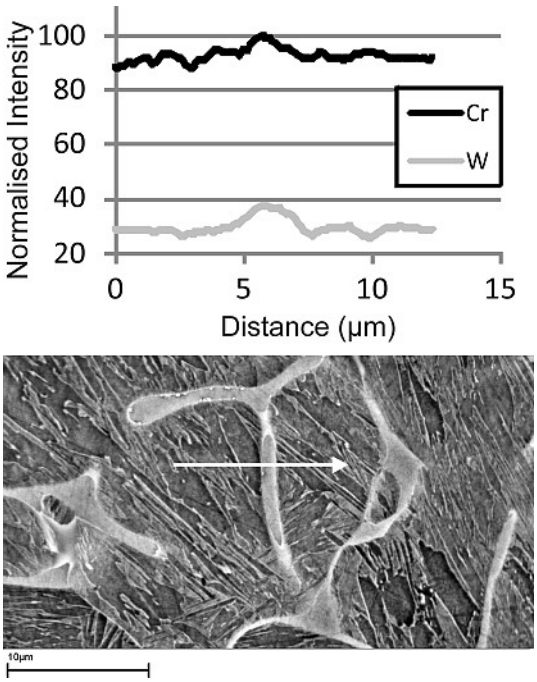

Fig. 7. EDX line scan across an elongated grain of delta ferrite showing local enrichment in chromium and tungsten.

pered martensite microstructure starts around 900 °C and ends at temperatures higher than 1016 °C, when the steel is fully austenitised. With a further increase in temperature of approximately 200 °C (1220 °C), the transformation of the austenite to delta ferrite is observed. On cooling, the major fraction of delta ferrite re-transforms to austenite, which then transforms to martensite after reaching the M_S temperature close to 430 °C. Small amounts of austenite and delta ferrite are retained, which leads to a final microstructure consisting of martensite with retained delta ferrite and retained austenite. For a heating rate of 100 K s^{-1}, the same sequence of phase transformations is observed, but transformation temperatures were not obtained.

2. Diffraction peak analysis of the XRD data was used to produce a quantitative phase evolution mapping as a function of the thermal cycle. The maximum amount of delta ferrite is measured shortly after reaching the peak temperature of 1300 °C close to 1250 °C. For the faster (100 K s^{-1}) thermal cycle, the maximum amount of delta ferrite is slightly lower with 45 % compared to 65 % of the slower (10 K s^{-1}) cycle. The levels of retained delta ferrite (4 %) as well as of retained austenite (4 %) within the HAZ simulated microstructure are similar for both thermal cycles.
3. During the simulated weld cycle, most of the precipitates are dissolved. Dissolution of chromium rich $M_{23}C_6$ particles along prior austenite grain boundaries as well as martensite lath and packet boundaries leads to local enrichment in chromium. This enrichment is high enough such that delta ferrite is stabilised down to room temperature. Electron microscopy and EDX measurements confirm this finding by clearly showing enrichment in chromium and tungsten in the delta ferrite grains.

The financial support of the Austrian Research Promotion Agency (FFG) within the project COST 536 ACCEPT is gratefully acknowledged. The LLNL portion of this work was performed under the auspices of the U.S. Department of Energy by Lawrence Livermore National Laboratory under Contract DE-AC52-07NA27344. The ORNL portion was sponsored by the Division of Materials Science and Engineering, U.S. Department of Energy through Contract DE-AC05-00OR22725 with the Oak Ridge National Laboratory. Work performed at the Advanced Photon Source (APS) is supported by the U.S. DOE under Award No. DEFG02-91ER45439, through the Frederick Seitz Materials Research Laboratory at the University of Illinois at Urbana-Champaign, the Oak Ridge National Laboratory (U.S. DOE contract DE-AC05-00OR22725 with UT-Battelle LLC), the National Institute of Standards and Technology (U.S. Department of Commerce) and UOP LLC. The APS is supported by the U.S. DOE, Basic Energy Sciences, Office of Science under contract No. W-31-109-ENG-38.

References

[1] P. Hofer, M.K. Miller, S.S. Babu, S.A. David, H. Cerjak: Metall. Mater. Trans. A 31 (2000) 975.
[2] M. Hättestrand, H.-O. Andrén: Mater. Sci. Eng. A 270 (1999) 33.
[3] F. Abe, T. Horiuchi, M. Taneike, K. Sawada: Mater. Sci. Eng. A 378 (2004) 299.
[4] S.K. Albert, M. Kondo, M. Tabuchi, F. Yin, K. Sawada, F. Abe: Metall. Mater. Trans. A 36 (2005) 333.
[5] E. El-Kashif, K. Asakura, K. Shibata: ISIJ International Vol. 40 No. 12 (2002) 1468.
[6] F. Abe, T. Horiuchi, K. Sawada: Mater. Sci. Forum 426–432 (2003) 1393.
[7] J. Hald, L. Korcakova: ISIJ International Vol. 43 No. 3 (2003) 420.
[8] L. Schäfer: Nucl. Mater. 258–263 (1998) 1336.
[9] J. Vekeman, A. Dhooge, S. Huysmans, B. Vandenberghe, C. Jochum: IIW Report XI-863-06 (2006).
[10] P.J. Grobner, W.C. Hagel: Metall. Trans. A Vol. A 11 (1980) 633.
[11] K. Sawada, H. Kushima, K. Kimura: ISIJ International Vol. 46(5) (2006) 769.
[12] M. Igarashi, M. Yoshizawa, in: R. Viswanathan, D. Gandy, K. Coleman (Eds.), 4th International Conference on Advances in Materials Technology for Fossil Power Plants, ASM International (2005).
[13] X.Y. Liu, T. Fujita: ISIJ International Vol. 29(8) (1989) 680.
[14] K. Kimura, K. Sawada, H. Kushima, Y. Toda, in: J. Lecomte–Beckers, M. Carton, F.Schubert, P.J. Ennis (Eds.), 8th International Conference on Materials for Advanced Power Engineering 2006, Forschungszentrum Jülich GmbH (2006).
[15] J.S. Park, S.J. Kim, C.S. Lee: Mater. Sci. Eng. A 298 (2001) 127.
[16] J.W. Baek, S.W. Nam, B.O. Kong, S.H. Ryu: Key Engineering Materials 297–300 (2005) 463.
[17] T. Hara, H. Asahi: ISIJ International Vol. 40(11) (2000) 1134.
[18] K. Easterling: Introduction to the physical metallurgy of welding, Butterworths (1983).
[19] H. Granjon: Fundamentals of Welding Metallurgy, Abington Publishing, Cambridge (1991).
[20] H. Cerjak, P. Mayr, in: F. Abe, T.U. Kern, V. Viswanathan (Eds.), Creep Reistant Steels, Woodhead Publishing, in print.
[21] J.W. Elmer, J. Wong, T. Ressler: Metall. Mater. Trans. A 29 (1998) 2761.
[22] J.W. Elmer, J. Wong, T. Ressler: Metall. Mater. Trans. A 32 (2001) 1175.
[23] T.A. Palmer, J.W. Elmer, J. Wong: Sci. Technol. Weld. 7 (2002) 159.
[24] J.W. Elmer, T.A. Palmer, W. Zhang, B. Wood, T. DebRoy: Acta Mater. 51 (2003) 3333.
[25] J.W. Elmer, T.A. Palmer, S.S. Babu, W. Zhang, T. Debroy: Welding Journal 83 (2004) 244.
[26] T.A. Palmer, J.W. Elmer: Metall. Mater. Trans. A 36 (2005) 3353.
[27] T.A. Palmer, J.W. Elmer: Scripta Mater 53 (2005) 535.
[28] J.W. Elmer, T.A. Palmer: Metall. Mater. Trans. A 37 (2006) 2171.
[29] J.W. Elmer, T.A. Palmer, S.S. Babu, E.D. Specht: Mater. Sci. Eng. A 391 (2005) 104.
[30] A.P. Hammersley: FIT2D V9.129 Reference Manual V3.1, ESRF Internal Report, ESRF98HA01T (1998).
[31] L. Xiao, Z. Fan, Z. Jinxiu, Z. Minxing, K. Mokuang, G. Zhenqi: Phys. Rev. 52 (1995) 9970.

(Received November 13, 2007; accepted January 21, 2008)

Bibliography

DOI 10.3139/146.101649
Int. J. Mat. Res. (formerly Z. Metallkd.)
99 (2008) 4; page ■ – ■
© Carl Hanser Verlag GmbH & Co. KG
ISSN 1862-5282

Correspondence address

Dr. Peter Mayr
Graz University of Technology
Institute for Materials Science, Welding and Forming
Kopernikusgasse 24, A-8010 Graz, Austria
Tel.: +43 316 873 7186
Fax: +43 316 873 7187
E-mail: peter.mayr@tugraz.at

You will find the article and additional material by entering the document number MK101649 on our website at www.ijmr.de